Imaging Reveals Importance of Shape and Flexibility for Glomerular Filtration of Biologics

Hanine Rafidi[1], Alberto Estevez[2], Gregory Z. Ferl[1,3], Danielle Mandikian[1], Shannon Stainton[4], Lauren Sermeño[1], Simon P. Williams[5], Amrita V. Kamath[1], James T. Koerber[5,6], and C. Andrew Boswell[1,3]

ABSTRACT

Advances in antibody engineering have enabled the construction of novel molecular formats in diverse shapes and sizes, providing new opportunities for cancer immunotherapeutic drug discovery while also revealing limitations in knowledge of structure–activity relationships. The current understanding of renal filtration originates largely from data reported for dextrans, IgG, albumin, and selected globular proteins. For a one-armed IgG-based T-cell imaging agent, we observed higher renal signal than typically observed for bivalent IgGs, prompting us to explore the factors governing renal filtration of biologics. We constructed a small representative library of IgG-like formats with varied shapes and hinge flexibilities falling broadly into two categories: branched molecules including bivalent IgG and $(scFv)_2$Fc, and nonbranched molecules including one-armed IgG, one-armed IgG with stacked Fab, and one-armed IgG with a rigid IgA_2 hinge. Transmission electron microscopy revealed Y-shaped structures for the branched molecules and pseudo-linear structures for the nonbranched molecules. Single-photon emission CT imaging, autoradiography, and tissue harvest studies demonstrated higher renal uptake and catabolism for nonbranched molecules relative to branched molecules. Among the nonbranched molecules, the one-armed IgG with rigid IgA_2 hinge molecule demonstrated higher kidney uptake and decreased systemic exposure relative to molecules with a more flexible hinge. Our results show that differences in shape and hinge flexibility drive the increased glomerular filtration of one-armed relative to bivalent antibodies and highlight the practical advantages of using imaging to assess renal filtration properties. These findings are particularly relevant for T-cell–dependent bispecific molecules, many of which have nonstandard antibody structures.

Introduction

The toolbox of molecular formats available for biologic drug development has greatly expanded beyond nonstandard IgG formats in the past decade due to advances in protein engineering and the need to achieve proper geometry for optimal cytolytic synapse formation in cancer immunotherapy (1). Several molecular structures, including single-armed formats, are being pursued for T-cell–dependent bispecific modalities. Given the availability of biologics in diverse sizes and shapes, it is important to understand how renal filtration affects systemic pharmacokinetic properties as well as undesirable kidney exposure, for example, in the case of a toxic or radioactive payload. In addition to being relevant in the pursuit of diagnostic imaging agents, renal filtration of biologics is also important for therapeutic applications in that it is often inversely proportional to the systemic exposure of the drug.

The structure and function of the glomerular filtration barrier (GFB) – particularly in terms of size and charge selectivity – has been widely studied, largely due to its clinical relevance to proteinuria (2). The degree to which the negatively charged glycocalyx contributes to the GFB has been widely debated, with some concluding that electrostatic charge plays a minor role secondary to that of size (3). While the glomerular endothelia within capillaries have fenestrae of approximately 50–150 nm in size (2), traversing molecules would encounter the glomerular basement membrane and kidney podocytes forming the glomerular slit diaphragm of approximately 4 nm (4) which is near the narrowest dimension of albumin ($\sim$67 kDa), an approximately 14×4 nm ellipsoid protein (5). However, the role of the glomerular slit has been questioned due to extensive permeation of albumin (and IgG to a lesser extent) into the lamina densa of the gel-like glomerular basement membrane and its accumulation upstream of the podocyte glycocalyx, although not upstream of the slit diaphragm itself (6). Even though some albumin traverses the GFB, very little of it ends up in the urine because it is either reclaimed by the neonatal Fc receptor (FcRn), or is reabsorbed, perhaps in a saturable manner, along the proximal tubules (6) by receptor-mediated endocytosis involving megalin and cubilin proteins (7) with a similar process occurring for peptides and antibody fragments (8).

Unlike many antibody fragments, the primary systemic clearance route of full-length IgG is not renal filtration but rather widespread fluid-phase pinocytosis into endothelial cells (9, 10). FcRn maintains serum protein homeostasis by preventing lysosomal degradation of Fc-containing immunoglobulins and albumin through a pH-dependent recycling mechanism in endothelial cells and is responsible for their long circulation half-lives (11). As a transcytosis receptor, FcRn serves multiple roles: removing IgG from the circulation into the renal

[1]Departments of Preclinical and Translational Pharmacokinetics and Pharmacodynamics, Genentech, Inc., South San Francisco, California. [2]Structural Biology, Genentech, Inc., South San Francisco, California. [3]Biomedical Imaging, Genentech, Inc., South San Francisco, California. [4]Safety Assessment, Genentech, Inc., South San Francisco, California. [5]Antibody Engineering, Genentech, Inc., South San Francisco, California. [6]Research and Early Development, Genentech, Inc., South San Francisco, California.

Corresponding Author: C. Andrew Boswell, Department of Preclinical and Translational Pharmacokinetics, Genentech, Inc., 1 DNA Way, MS 463A, South San Francisco, CA 94080. E-mail: boswell.andy@gene.com

interstitium via vascular endothelial cells, reclaiming albumin from the kidney ultrafiltrate in proximal tubule endothelial cells, and facilitating the urinary clearance of IgG that traversed the GFB in podocytes (12).

While electron microscopy is the classical method for high-resolution imaging of the GFB (3, 6), nuclear imaging methods such as single-photon emission CT (SPECT) provide a rapid, noninvasive method for assessing levels of filtration/reabsorption on a whole-kidney basis. For diagnostic imaging agents, achieving ideal pharmacokinetics often requires a rapid "washout" from circulation to enable high signal-to-background ratios on a same-day timespan. Pursuit of such tracers has prompted the study of a variety of molecular sizes, including $F(ab')_2$ (~110 kDa; refs. 13, 14), $(scFv)_2Fc$ with mutations to ablate FcRn binding (~105 kDa; ref. 15), minibodies (~80 kDa; ref. 16), diabodies (~55 kDa; ref. 17), Fabs (~50 kDa; refs. 14, 18), and nanobodies (~15 kDa; ref. 19). High renal signal is evident when imaging with antibody fragments, particularly when using residualizing (radio-metal-chelate) labels (20), due to retention within renal proximal tubules following reabsorption and lysosomal degradation (8). Importantly, comparisons across molecules of varying sizes should be restricted to molecules that do, or do not, bind FcRn.

We observed that a one-armed IgG (113 kDa), a format pursued for cancer therapy (21) and more recently for diagnostic

Figure 1.
Selective passage of biologic imaging agents across the glomerular filtration barrier. Structural depiction of glomerular filtration for radiolabeled IgG-based imaging agents and antibodies. Antibodies flow through glomerular capillaries and are filtered through endothelial fenestrae (glomerular basement membrane and podocytes not shown for simplicity). One-armed IgG crosses the glomerular filtration barrier more readily than IgG, leading to reabsorption from ultrafiltrate, lysosomal degradation, and subsequent buildup of radioactive catabolites within renal proximal tubule cells.

purposes (22–24), was more susceptible to glomerular filtration and tubular reabsorption *in vivo* relative to conventional (bivalent) IgG (**Fig. 1**). We hypothesized that the unbranched, narrow and pseudolinear shape of one-armed IgG will facilitate its renal filtration and passage through the GFB. We further hypothesized that the increased flexibility of one-armed molecules – owing to the absence of steric hindrance between two Fab arms – would allow greater degrees of freedom to adopt conformations that are susceptible to glomerular filtration. In contrast, the branched IgG's two Fab arms may limit its ability to adopt linear or compact shapes, thus contributing to its exclusion from glomerular filtration. To that end, we synthesized a small library of IgG-like formats (see Supplementary Table S1 for sequences) varying in shape and hinge flexibility: conventional IgG (156 kDa), one-armed IgG (113 kDa), $(scFv)_2Fc$ (115 kDa), one-armed IgG with a stacked Fab (159 kDa), and a one-armed IgG with a rigid IgA_2 hinge (ref. 25; 106 kDa). The similar molecular weight ranges of 106–115 and 156–159 kDa should allow for comparison of shape/structure between selected molecules with negligible differences in size. All antibodies contained an intact Fc region for FcRn binding/recycling and recognized a herpes simplex virus glycoprotein D (gD) epitope (i.e., anti-gD) that is not present in mice to circumvent any confounding effect of target binding in our study interpretation. Transmission electron microscopy (TEM) provided images of representative structural confirmations of these variants. Subsequent SPECT imaging allowed comprehensive assessment of the *in vivo* glomerular filtration of all variants.

Materials and Methods

Antibody engineering and characterization

To generate each format, we designed light chain and heavy chain constructs using anti-HSV1 glycoprotein D antibody (Supplementary Table S1). Constructs were synthesized and subcloned into mammalian expression vectors (Genewiz). All Fcs were hIgG1 that contain L234A, L235A, and P329A (LALAPG) to remove effector function (26). The Fc portions of the one-armed antibodies contain the knobs-into-holes mutations to facilitate bispecific assembly (27). All antibodies were expressed by transient transfection of 293 cells. DNA encoding for the three chains of each one-armed antibody were mixed at a 2:1:1 ratio (LC1:HC1:HC2). Antibodies were purified by affinity chromatography and size-exclusion chromatography (SEC) using standard methods (MabSelect SuRe; GE Healthcare).

The absolute molar mass and hydrodynamic radius were determined by size-exclusion chromatography and multi-angle light scattering (SEC-MALS) analysis. Briefly, an aliquot of each antibody in PBS was loaded onto a BEH XBridge SEC column (Waters) on a Dionex Ultimate 3000 instrument (Thermo Scientific). MALS analysis was performed using a miniDAWN TREOS (Wyatt Technology). Nonspecific binding of each anti-gD antibody variant was evaluated using a previously described ELISA with baculovirus particles (BV-ELISA; ref. 28).

Negative stain TEM

All 5 samples were treated identically for the negative staining procedure. Samples were diluted to a concentration of 0.01 mg/mL then 4 µL was deposited and incubated (for a minimum of 30 seconds) on a glow-discharge using a Glo-Cube plasma cleaner (Quarum) on ultra-thin carbon coated 400-mesh copper grid (Electron Microscopy Sciences). Following incubation, the sample was negatively stained by touching the protein bound side of the grid serially onto 5 drops (40 µL
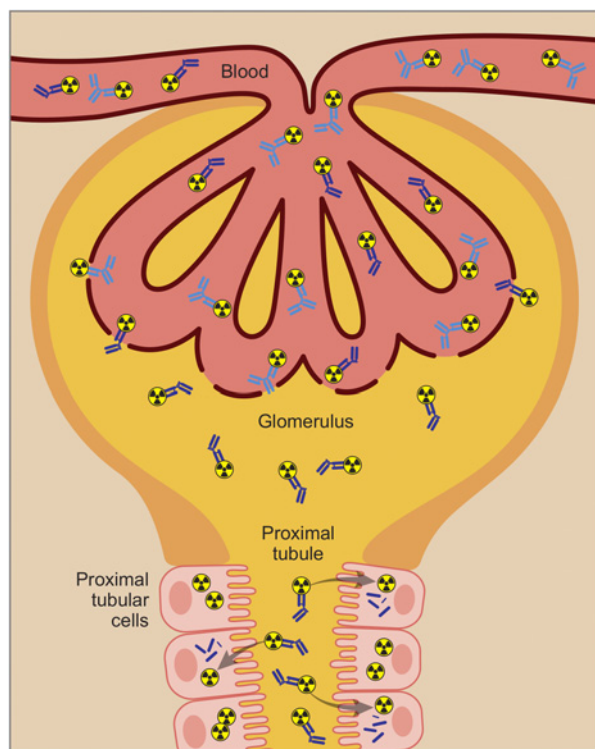
each drop) of 2% uranyl acetate (Electron Microscopy Sciences) and placed on a parafilm working surface. Excess stain was allowed to sit on the grid for >30 seconds and then wicked away using #1 Whatman filter paper. Imaging was performed on a Talos 200C equipped with 4K Ceta-D, CMOS camera (Thermo Fisher Scientific), at a magnification of 57k. Resulting micrographs were then processed in cisTEM image analysis software (cisTEM.org) to produce 2D class averages from which overall structure can be observed.

Radiochemistry

Radiosynthesis of ^{111}In-labeled proteins was achieved through incubation of ^{111}InCl$_3$ and 1,4,7,10-tetraazacyclododecane-1,4,7,10-tetraacetic acid (DOTA)-conjugated (randomly through lysines) proteins in 0.3 mol/L ammonium acetate pH 7 at 37°C for 1 hour. Radiosynthesis of ^{125}I-labeled proteins was achieved through indirect iodination through tyrosine residues (29). Purification of all radioimmunoconjugates was achieved using NAP-5 columns equilibrated in PBS and confirmed by size-exclusion chromatography. *In vitro* stability was assessed by incubation of all five molecules in mouse plasma at 37°C followed by size-exclusion chromatography.

SPECT-CT imaging

All animal experiments were conducted in accordance with, and with approval of, the American Association for Accreditation of Laboratory Animal Care and the Genentech Institutional Animal Care and Use Committee (IACUC). The SCID-Beige mouse model was chosen to allow comparison with our previous PET imaging data in tumor-bearing mice of the same strain involving a single-arm anti-CD8 antibody alongside its nonbinding anti-gD control (24). SCID-Beige mice were dosed intravenously via tail vein with 300 μCi of ^{111}In-labeled protein that was adjusted with unlabeled protein to a 5 mg/kg total dose. SPECT images were acquired in two 20% windows centered at the 173- and 247-keV photopeaks of ^{111}In using an ultra-high sensitivity mouse 2.0-mm-pinhole collimator (MILabs). Three frames (15 minutes each) were acquired. Image reconstruction and coregistration was performed using MILabs software, and SPECT visualization was performed using VivoQuant. Tracer concentrations in blood and kidney were extracted from the SPECT scans by drawing regions of interest (ROI) on the corresponding, coregistered CT scans, where the heart was used for a surrogate for blood and the portion of kidney visible in the CT scan was assumed to be representative of whole kidney. The median SPECT signal intensity was extracted from each ROI and used to calculate kidney:blood ratios, which were compared with cut-and-count based kidney:blood ratios when available to validate the approach. Image processing and quantification was performed using Amira visual data analysis software (version 6.2; FEI Co.) and MATLAB (R2018b; version 9.5.0.944444; The Mathworks Inc.).

Whole-body autoradiography

Animals were embedded in 3% carboxymethylcellulose and stored at −80°C for 24–48 hours. Twenty-micron–thick sagittal sections were obtained using a cryostat microtome (CM3600; Leica) at −20°C. Sections were mounted on clear tape and lyophilized for approximately 24 hours. The whole-body cryosections were covered with Mylar film and exposed at room temperature to phosphor-imaging plates (YBIP 2025MS; Fuji Film Medical Systems, Inc.) for 24–48 hours and were then scanned using a Fuji Film BAS-5000 scanner (Fuji Film Medical Systems, Inc.).

Pharmacokinetics and biodistribution

All animal experiments were conducted in accordance with, and approval of, the American Association for Accreditation of Laboratory Animal Care and the Genentech Institutional Animal Care and Use Committee (IACUC). Biodistribution studies were performed in female SCID-Beige mice (3 per group; 6–8 weeks old) administered with an intravenous bolus of ^{125}I-labeled and ^{111}In-labeled antibody tracers (5 μCi each) with the respective unmodified antibody for a total dose of 5 mg/kg. Blood samples were collected from each animal at 0.25, 1, and 2 days to derive plasma and whole-blood antibody concentrations. At 2 days, tissue samples were collected by terminal organ harvest and counted for radioactivity using a 1480 WIZARD Gamma Counter in the energy windows for ^{111}In (245 keV; decay $t_{1/2}$ = 2.8 days) and ^{125}I (35 keV; decay $t_{1/2}$ = 59.5 days) with automatic background and decay correction. Catabolism can be approximated as the difference between ^{111}In (intact plus residualized) and ^{125}I (intact only) signals (30, 31). However, this method does not provide a perfect readout of catabolism for all organs, particularly for those with fast cell turnover rates or those containing high levels of dehalogenase enzymes.

A standard, linear two-compartment pharmacokinetic model was fitted simultaneously to all blood sample–derived pharmacokinetic data, where the central distribution volume (V_1) was estimated but forced to be equal across all molecules and individual values of elimination clearance (CL), peripheral distribution volume (V_2), and distribution clearance (CL_d) were estimated for each molecule. Model fitting was performed using MATLAB SimBiology (R2018b; The MathWorks Inc.).

Results

Antibody engineering and characterization

We analyzed differences in molecular size and shape using SEC-MALS and observed similar hydrodynamic radii for the IgG and one-armed IgG with stacked Fab and a smaller hydrodynamic radius for the other three formats (Supplementary Table S2). No significant differences in theoretical isoelectric point (pI) values were noted among the various parental molecules, and the number of DOTA moieties added per antibody on a molar basis was low and roughly consistent (1.1–2.4) across molecules as measured by mass spectrometry (Supplementary Table S2). In addition, no significant differences in baculovirus (BV) ELISA scores were noted across all five molecules, and all scores were below the cutoff (<5) for concerns around non-specific binding (Supplementary Table S2).

Negative stain TEM

A schematic of each format used in this study is depicted alongside its TEM image (**Fig. 2A–E**). TEM showed the expected branched, Y-shaped structure for the bivalent IgG (**Fig. 2A**) and a similar but shorter branched structure for the (scFv)$_2$Fc (**Fig. 2B**). Images for the remainder of the one-armed antibodies revealed unbranched, continuous structures (**Fig. 2C–E**).

Radiochemistry

Specific activities were 5.3–15.5 μCi/μg for ^{111}In-labeling and 7.6–9.5 μCi/μg for ^{125}I-labeling. Size-exclusion radiochromatograms for all five ^{111}In-DOTA-labeled and ^{125}I-labeled molecules are shown in Supplementary Fig. S1 demonstrating that virtually all radiometal/radioiodine is incorporated into the immunoconjugate (i.e., radiochemical purity). Furthermore, these molecules were checked for plasma stability and showed no evidence of low molecular weight
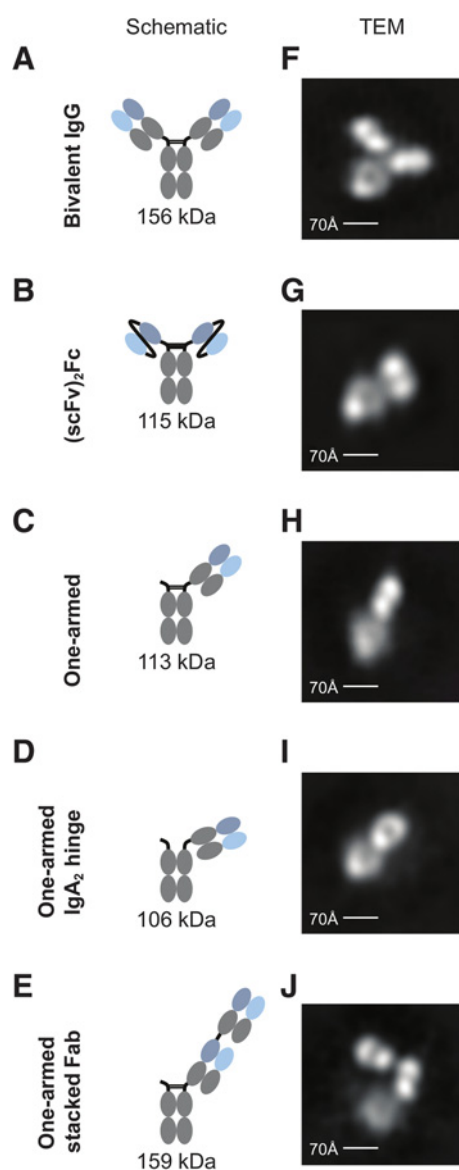
Figure 2.
Structural analysis using negative stain transmission electron micrographs. Structural cartoon schematics of bivalent and one-armed antibody molecules studied with their corresponding TEM images: bivalent IgG (**A, F**), (scFv)$_2$Fc (**B, G**), one-armed IgG (**C, H**), one-armed IgG with IgA$_2$ hinge (**D, I**), and one-armed IgG with stacked Fab (**E, J**).

radioactive species after plasma incubation (at 37°C) for 1 day (Supplementary Fig. S2).

SPECT-CT imaging

SPECT imaging performed at 6, 24, and 48 hours post-intravenous injection of radiolabeled antibodies revealed a wide range of blood pool and kidney SPECT signals (**Fig. 3A–E**). There was little to no difference in disposition between the two branched molecules - bivalent IgG (**Fig. 3A**) and (scFv)$_2$Fc (**Fig. 3B**), with the majority of the signal residing within the blood pool (heart, jugular veins, and vena cava) and gradually decreasing over two days with no visible kidney uptake/delineation. In striking contrast, notable kidney

uptake was evident as early as 6 hours for all one-armed antibodies (**Fig. 3C–E**). By day two, further renal signal accumulation was evident for one-armed antibodies and delineation of blood pool, primarily heart and vena cava, revealed roughly similar systemic concentrations for all formats except for the IgA$_2$ rigid-hinge one-armed antibody, whose high kidney uptake appeared to have resulted in diminished exposure (**Fig. 3D**).

We compared SPECT image-derived kidney uptake for the (scFv)$_2$Fc and the one-armed IgG formats (both ~100 kDa) to test the hypothesis that two molecules with a similar molecular weight, but different branching structures, may have different renal uptake patterns. The one-armed IgG showed significant kidney uptake with 1.7, 3.0, and 2.7-fold higher SPECT signal than (scFv)$_2$Fc (and 1.5, 2.5, and 3.3-fold higher than IgG) at 6, 24, and 48 hours, respectively (**Fig. 3**; Supplementary Table S3). To gain further insight, we also compared the one-armed IgG with stacked Fab to the conventional IgG format (both ~150 kDa). The one-armed IgG with stacked Fab had 1.3, 2.0, and 2.1-fold higher kidney uptake relative to IgG at 6, 24, 48 hours, respectively, demonstrating differential renal uptake despite similar molecular weight. Taking advantage of the rigidity of the IgA$_2$ hinge region, we further explored whether hinge flexibility plays an important role in the level of renal filtration. The one-armed IgG with an IgA$_2$ hinge had 1.3, 1.8 and 2.2-fold higher kidney uptake than one-armed IgG (and 2.0, 4.6, and 7.1-fold higher than IgG) at 6, 24, and 48 hours respectively (**Fig. 3**; Supplementary Table S3).

Whole-body autoradiography

To visualize renal uptake with higher resolution, animals were sacrificed after SPECT image acquisition, and sagittal cryo-sections were obtained. The bright field images with their corresponding whole body autoradiographs (**Fig. 4A–E**) demonstrated cortical localization of radioactivity for one-armed antibodies, with far less medullary signal, consistent with reabsorption and degradation within proximal tubular cells within the kidney cortex (8). The same approximate rank order of kidney uptake as obtained by SPECT was qualitatively evident: one-armed IgG IgA$_2$ hinge >> one-armed IgG > one-armed IgG with stacked Fab > bivalent IgG ~ (scFv)$_2$Fc.

Pharmacokinetics and biodistribution

A separate group of mice designated for terminal tissue harvest with subsequent radioactive gamma counting (but no imaging) provided an orthogonal quantitative comparison of kidney uptake values. This dual isotope biodistribution study employed a mixture of halogen (^{125}I via tyrosines) and residualizing metal chelate (^{111}In-DOTA via lysines) labels to distinguish between intact and catabolized signals (20). Two-day blood concentrations (^{111}In signal) ranged from 18–22%ID/mL for all molecules except the one-armed IgA$_2$ hinge, which was 13%ID/mL (**Fig. 5A–B**). Concordantly, the lowest AUC value was 36.6 day %ID/mL for the one-armed IgA$_2$ hinge while the others ranged from 46.0–55.4 day %ID/mL (Supplementary Table S4) demonstrating that the strong kidney uptake for this molecule affected its exposure.

Among the five molecules evaluated, little to no catabolism (filled portion of bars) was evident in whole blood, liver and muscle (**Fig. 5B**). Catabolized signal in the kidney was variable, with 3.2, 4.0, 26.5, 73.0, and 15.6%ID/g for IgG, (scFv)$_2$Fc, one-armed IgG, one-armed IgG with IgA$_2$ hinge, and one-armed IgG with stacked Fab, respectively. A correlation plot analysis of kidney to blood ratios (**Fig. 5C**) demonstrated agreement between the

Rafidi et al.
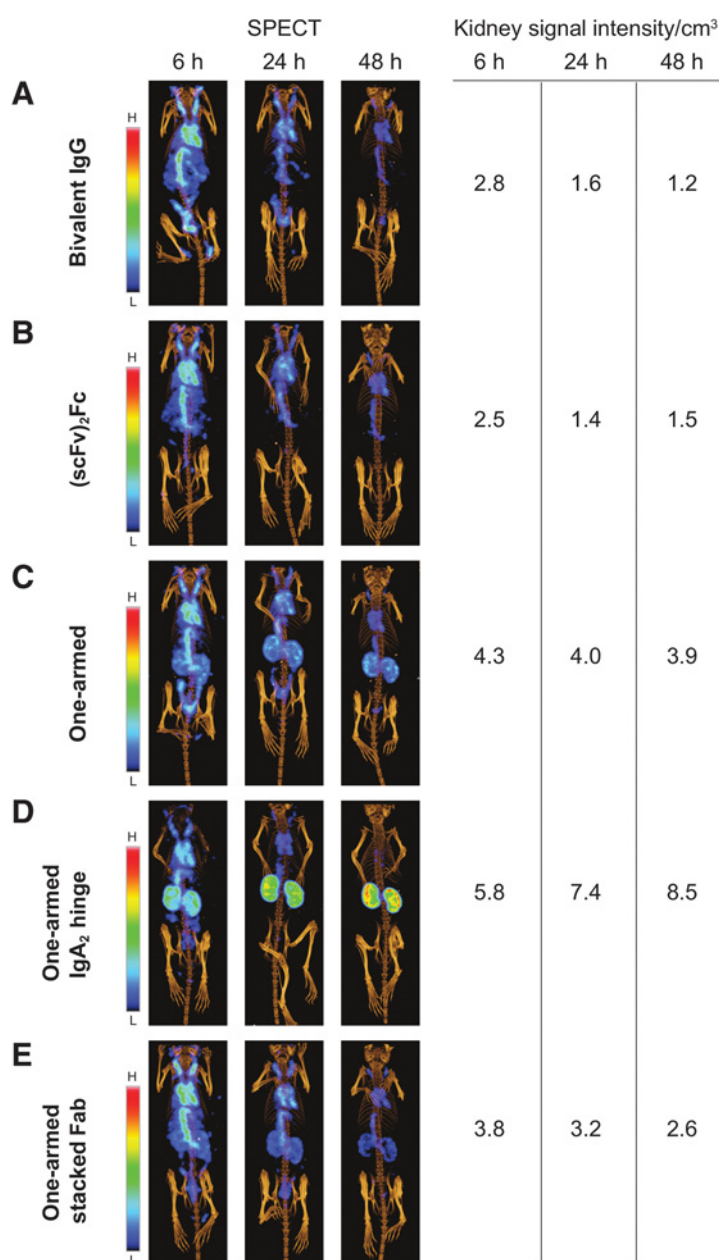
Figure 3.
In vivo longitudinal SPECT imaging. Mice were injected intravenously with various ^{111}In-DOTA-labeled antibodies and imaged using SPECT-CT at 6, 24, and 48 hours for bivalent IgG (**A**), (scFv)$_2$Fc (**B**), one-armed IgG (**C**), one-armed IgG with IgA$_2$ hinge (**D**), and one-armed IgG with stacked Fab (**E**). SPECT images are scaled consistently across all images in units of intensity per cm^3. The color scales are labeled as "L" (low; equivalent to ~7%ID/g) to "H" (high; equivalent to ~80%ID/g).

imaging data (**Figs. 3** and **4**) and the tissue/blood harvest data (**Fig. 5A** and **B**). Biodistribution data for additional tissues can be found in Supplementary Fig. S3. Nonperfused kidney homogenates were analyzed in an independent study, and the radioactive signal was confirmed to be associated with a low molecular weight species for one-armed IgG, whereas only intact antibody (likely within the blood pool) was detected for IgG (Supplementary Fig. S4).

Discussion

We initially observed that one-armed antibody-based imaging agents revealed a more intense imaging signal in kidneys than their bivalent counterparts (22–24). On the basis of this data, we hypothesized that one-armed antibodies are far more susceptible to apparent glomerular filtration and degradation (**Fig. 1**). This phe-

nomenon could be explained by considering antibodies not as singular spherical proteins but rather as smaller proteins (Fabs and Fcs) – molecules known to cross the glomerular barrier individually – tethered together. To explore structure–activity relationships governing the renal handling of biologics in finer detail, we engineered a series of Fc-containing antibodies of various shapes and sizes, all having the same (nonexpressed) antigen so that only physicochemical properties – and not specific targeting – would affect glomerular filtration. Furthermore, we chose to monitor renal filtration using a convenient noninvasive imaging modality (SPECT) paired with a radiometal-chelate probe to capture both intact and degraded protein. Detection of solely intact antibody by ELISA or mass spectrometry would not have captured the differences in renal filtration and degradation that our residualizing (^{111}In) SPECT imaging method has revealed.
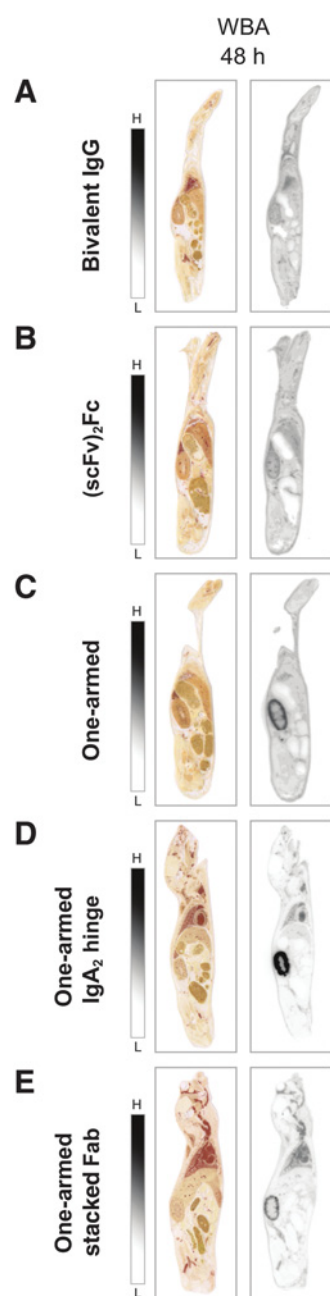
Figure 4.
Whole-body autoradiographic (WBA) imaging. Autoradiographic images are shown for for bivalent IgG (**A**), (scFv)₂Fc (**B**), one-armed IgG (**C**), one-armed IgG with IgA₂ hinge (**D**), and one-armed IgG with stacked Fab (**E**). After the last SPECT-CT acquisition at 48 hours, mice were euthanized and processed for WBA to obtain sagittal sections that include the major organs. Sections were exposed to phosphor-imaging film for 24 to 48 hours.

TEM imaging allowed shape assessment of each molecule (**Fig. 2A–E**) and revealed that, for each molecule found to exhibit a Y-shaped conformation, little to no renal uptake was observed by SPECT imaging (**Fig. 3A–E**) or by autoradiography (**Fig. 4A–E**). In fact, in this limited data set, discriminating between branched versus unbranched molecules by TEM seems to be a better predictor

of renal filtration than the SEC-MALS data (Supplementary Table S2). However, neither TEM nor SEC-MALS fully capture the asymmetry of molecules in solution, and other techniques for separating based shape and/or size (e.g., native gel electrophoresis or ultracentrifugation) do not capture the physiological complexities of the GFB. This lends to the importance of why SPECT imaging is a valuable tool in pharmacokinetic characterization, particularly for monitoring renal uptake and catabolism, of biologic molecules.

Quantitative assessment of kidney uptake by tissue harvest revealed lower blood exposure (**Fig. 5A**) and higher kidney uptake (**Fig. 5B**) for the one-armed antibody having a rigid IgA₂ hinge than with the standard hinge. We had initially anticipated that a rigid hinge might reduce glomerular filtration by restricting the range of motion needed to assume a conformation that can pass across the GFB. However, to our surprise the opposite trend was observed, perhaps suggesting that locking the one-armed antibody into a long, rigid, and narrow conformation allowed it to be filtered more readily than its counterpart with a standard, flexible IgG hinge. Indeed, the idea that "deformability" may play a role in glomerular permselectivity has arisen in the context that dextrans are more linear and flexible molecules – thus more susceptible to filtration – relative to globular proteins (32).

Understanding the molecular species associated with the visualized radioactive signal is critical for interpreting imaging data. We used size-exclusion chromatography to demonstrate that, for the one-armed antibody, the elevated radioactive signal in kidney homogenates was associated with a low-molecular weight species (Supplementary Fig. S4). Importantly, several investigations including analyses of urine samples from clinical trials demonstrate that [¹¹¹In]DOTA-ε-amino-lysine is the major radioactive catabolite of ¹¹¹In-DOTA-modified antibodies and, when injected intravenously into mice, this catabolite rapidly cleared into the urine without kidney retention (33). These observations, along with the residualizing properties of [¹¹¹In]DOTA-ε-amino-lysine, strongly favor the intracellular production and trapping of this catabolite within renal proximal tubules as opposed to redistribution of this catabolite from other tissues.

We chose to execute our studies using a residualizing (radiometal) probe so that we can capture a snapshot of this rapid physiologic process in time by monitoring renal accumulation of the trapped catabolites rather than the intact molecules themselves. The similarity in ¹²⁵I (intact) levels among the five IgG constructs was expected because the processes of reabsorption, lysosomal degradation, and whole-body excretion of ¹²⁵I-containing catabolites occur so rapidly following renal filtration that the levels of intact antibody remain constantly low and indistinguishable from one another. In fact, ¹²⁵I levels of branched molecules in (nonperfused) kidneys are slightly higher than that of unbranched molecules, reflecting higher systemic exposures. While dehalogenation has been a general concern for radioiodinated proteins *in vivo*, previous work has suggested little to no differences among an ¹²⁵I-labeled IgG, F(ab')2 and Fab when labeled by electrophilic addition to tyrosines (similar to the current method) versus labeling through lysines using a dehalogenase-resistant method (34).

Conclusions

In conclusion, we evaluated molecular formats differing in size, shape and hinge flexibility to explore structure-activity relationships governing the glomerular filtration and catabolism of biologics. Our *in vivo* studies of one-armed IgG, one-armed IgG with stacked Fab, and one-armed IgG with a rigid IgA₂ hinge demonstrated glomerular filtration and subsequent catabolism within renal proximal tubules.
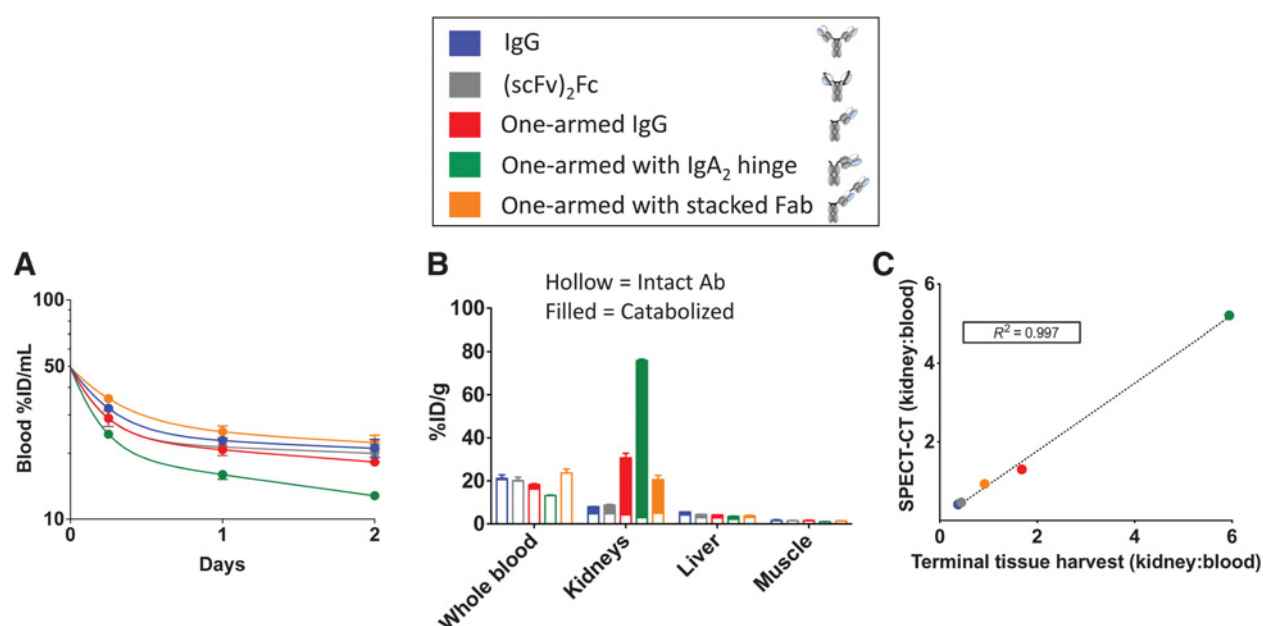
Figure 5.
Pharmacokinetics and tissue biodistribution of antibody variants. **A,** Time–activity curves depicting blood pharmacokinetics expressed in units of percentage of injected radioactive dose per mL of blood (%ID/mL). Pharmacokinetic model fits were forced to an extrapolated blood concentration of 50%ID/mL at time zero based on 100% of the injected dose divided by an average mouse blood volume of approximately 2 mL. **B,** Tissue uptake expressed in units of percentage of injected radioactive dose per gram of tissue (%ID/g). Hollow portions of bars represent intact protein (measured by ^{125}I), whereas filled portions of bars represent catabolized protein (approximated as ^{111}In minus ^{125}I). **C,** Correlation plot demonstrating that kidney-to-blood ratios agree between SPECT (*y*-axis) and invasive biodistribution (*x*-axis) studies.

In contrast, IgG and (scFv)₂Fc were largely excluded from renal filtration/catabolism, possibly owing to the branched structures of these molecules as revealed by TEM. The variant with the rigid IgA₂ hinge produced the highest kidney signal, highlighting the importance of hinge flexibility. Overall, our results emphasize the practical advantages of imaging in the assessment of antibody distribution properties and demonstrate that shape and hinge flexibility drive the increased glomerular filtration of one-armed relative to bivalent antibodies. These findings highlight differences in renal distribution and systemic exposure between differently shaped molecules which may have important implications in the efficacy and safety profiles of cancer immunotherapeutic candidates.

Authors' Disclosures

D. Mandikian reports being an employee of Genentech, Inc., being a member of the Roche group, and owning Roche stock and/or options. A.V. Kamath reports personal fees from Genentech, Inc., outside the submitted work. J.T. Koerber reports being a current employee of Genentech, Inc. C. Boswell reports being an employee of Genentech, Inc., being a member of the Roche group, and owning Roche stock and/or options. No disclosures were reported by the other authors.

Authors' Contributions

H. Rafidi: Data curation, validation, investigation, methodology, writing–original draft. **A. Estevez:** Data curation. **G.Z. Ferl:** Data curation. **D. Mandikian:** Conceptualization, investigation. **S. Stainton:** Data curation. **L. Sermeño:** Visualization. **S.P. Williams:** Supervision. **A.V. Kamath:** Supervision. **J.T. Koerber:** Data curation. **C.A. Boswell:** Conceptualization, supervision.

References

1. Brinkmann U, Kontermann RE. The making of bispecific antibodies. mAbs 2017; 9:182–212.
2. Haraldsson B, Nystrom J, Deen WM. Properties of the glomerular barrier and mechanisms of proteinuria. Physiol Rev 2008;88:451–87.
3. Miner JH. The glomerular basement membrane. Exp Cell Res 2012;318:973–8.
4. Wartiovaara J, Öfverstedt L-G, Khoshnoodi J, Zhang J, Mäkelä E, Sandin S, et al. Nephrin strands contribute to a porous slit diaphragm scaffold as revealed by electron tomography. J Clin Invest 2004;114:1475–83.
5. Comper WD, Glasgow EF. Charge selectivity in kidney ultrafiltration. Kidney Int 1995;47:1242–51.
6. Lawrence MG, Altenburg MK, Sanford R, Willett JD, Bleasdale B, Ballou B, et al. Permeation of macromolecules into the renal glomerular basement membrane and capture by the tubules. Proc Natl Acad Sci 2017;114:2958–63.
7. Gekle M. Renal tubule albumin transport. Annu Rev Physiol 2005;67:573–94.
8. Vegt E, de Jong M, Wetzels JF, Masereeuw R, Melis M, Oyen WJ, et al. Renal toxicity of radiolabeled peptides and antibody fragments: mechanisms, impact

on radionuclide therapy, and strategies for prevention. J Nucl Med 2010;51: 1049–58.

9. Ryman JT, Meibohm B. Pharmacokinetics of monoclonal antibodies. CPT Pharmacometrics Syst Pharmacol 2017;6:576–88.

10. Tabrizi M, Bornstein GG, Suria H. Biodistribution mechanisms of therapeutic monoclonal antibodies in health and disease. AAPS J 2010;12:33–43.

11. Roopenian DC, Akilesh S. FcRn: the neonatal Fc receptor comes of age. Nat Rev Immunol 2007;7:715–25.

12. Sarav M, Wang Y, Hack BK, Chang A, Jensen M, Bao L, et al. Renal FcRn reclaims albumin but facilitates elimination of IgG. J Am Soc Nephrol 2009;20:1941–52.

13. Sham JG, Kievit FM, Grierson JR, Chiarelli PA, Miyaoka RS, Zhang M, et al. Glypican-3-targeting F(ab')2 for [89]Zr PET of hepatocellular carcinoma. J Nucl Med 2014;55:2032–7.

14. Heskamp S, van Laarhoven HW, Molkenboer-Kuenen JD, Bouwman WH, van der Graaf WT, Oyen WJ, et al. Optimization of IGF-1R SPECT/CT imaging using ^{111}In-labeled F(ab')2 and Fab fragments of the monoclonal antibody R1507. Mol Pharm 2012;9:2314–21.

15. Kenanova V, Olafsen T, Williams LE, Ruel NH, Longmate J, Yazaki PJ, et al. Radioiodinated versus radiometal-labeled anti-carcinoembryonic antigen single-chain Fv-Fc antibody fragments: optimal pharmacokinetics for therapy. Cancer Res 2007;67:718–26.

16. Olafsen T, Kenanova VE, Sundaresan G, Anderson AL, Crow D, Yazaki PJ, et al. Optimizing radiolabeled engineered anti-p185HER2 antibody fragments for in vivo imaging. Cancer Res 2005;65:5907–16.

17. Olafsen T, Sirk SJ, Olma S, Shen CK, Wu AM. ImmunoPET using engineered antibody fragments: fluorine-18 labeled diabodies for same-day imaging. Tumour Biol 2012;33:669–77.

18. Chakravarty R, Goel S, Valdovinos HF, Hernandez R, Hong H, Nickles RJ, et al. Matching the decay half-life with the biological half-life: ImmunoPET imaging with [44]Sc-labeled cetuximab Fab fragment. Bioconjug Chem 2014;25:2197–204.

19. Xavier C, Vaneycken I, D'Huyvetter M, Heemskerk J, Keyaerts M, Vincke C, et al. Synthesis, preclinical validation, dosimetry, and toxicity of ^{68}Ga-NOTA-anti-HER2 Nanobodies for iPET imaging of HER2 receptor expression in cancer. J Nucl Med 2013;54:776–84.

20. Boswell CA, Marik J, Elowson MJ, Reyes NA, Ulufatu S, Bumbaca D, et al. Enhanced tumor retention of a radiohalogen label for site-specific modification of antibodies. J Med Chem 2013;56:9418–26.

21. Merchant M, Ma X, Maun HR, Zheng Z, Peng J, Romero M, et al. Monovalent antibody design and mechanism of action of onartuzumab, a MET antagonist with anti-tumor activity as a therapeutic agent. Proc Natl Acad Sci U S A 2013; 110:E2987–96.

22. Klingler S, Fay R, Holland JP. Light-induced radiosynthesis of [89]ZrDFO-azepin-onartuzumab for imaging the hepatocyte growth factor receptor. J Nucl Med 2020;61:1072–8.

23. Fay R, Gut M, Holland JP. Photoradiosynthesis of ^{68}Ga-Labeled HBED-CC-azepin-MetMAb for immuno-PET of c-MET receptors. Bioconjug Chem 2019; 30:1814–20.

24. Gill H, Seipert R, Carroll VM, Gouasmat A, Yin J, Ogasawara A, et al. The production, quality control, and characterization of ZED8, a CD8-Specific [89]Zr-labeled immuno-PET clinical imaging agent. AAPS J 2020;22:22.

25. Roux KH, Strelets L, Brekke OH, Sandlie I, Michaelsen TE. Comparisons of the ability of human IgG3 hinge mutants, IgM, IgE, and IgA2, to form small immune complexes: a role for flexibility and geometry. J Immunol 1998;161: 4083–90.

26. Schlothauer T, Herter S, Koller CF, Grau-Richards S, Steinhart V, Spick C, et al. Novel human IgG1 and IgG4 Fc-engineered antibodies with completely abolished immune effector functions. Protein Eng Des Sel 2016;29:457–66.

27. Ridgway JB, Presta LG, Carter P. Knobs-into-holes' engineering of antibody CH3 domains for heavy chain heterodimerization. Protein Eng 1996; 9:617–21.

28. Hötzel I, Theil FP, Bernstein LJ, Prabhu S, Deng R, Quintana L, et al. A strategy for risk mitigation of antibodies with fast clearance. MAbs 2012;4:753–60.

29. Chizzonite R, Truitt T, Podlaski FJ, Wolitzky AG, Quinn PM, Nunes P, et al. IL-12: monoclonal antibodies specific for the 40-kDa subunit block receptor binding and biologic activity on activated human lymphoblasts. J Immunol 1991;147: 1548–56.

30. Perera RM, Zoncu R, Johns TG, Pypaert M, Lee FT, Mellman I, et al. Internalization, intracellular trafficking, and biodistribution of monoclonal antibody 806: a novel anti-epidermal growth factor receptor antibody. Neoplasia (New York, NY) 2007;9:1099–110.

31. Boswell CA, Bumbaca D, Fielder PJ, Khawli LA. Compartmental tissue distribution of antibody therapeutics: experimental approaches and interpretations. AAPS J 2012;14:612–8.

32. Venturoli D, Rippe B. Ficoll and dextran vs. globular proteins as probes for testing glomerular permselectivity: effects of molecular size, shape, charge, and deformability. Am J Physiol Ren Physiol 2005;288:F605–13.

33. Tsai SW, Li L, Williams LE, Anderson AL, Raubitschek AA, Shively JE. Metabolism and renal clearance of ^{111}In-labeled DOTA-conjugated antibody fragments. Bioconjug Chem 2001;12:264–70.

34. Wilbur DS, Hadley SW, Hylarides MD, Abrams PG, Beaumier PA, Morgan AC, et al. Development of a stable radioiodinating reagent to label monoclonal antibodies for radiotherapy of cancer. J Nucl Med 1989;30:216–26.

Molecular Cancer Therapeutics

Imaging Reveals Importance of Shape and Flexibility for Glomerular Filtration of Biologics

Hanine Rafidi, Alberto Estevez, Gregory Z. Ferl, et al.

Updated version	Access the most recent version of this article at: doi:10.1158/1535-7163.MCT-21-0116
Supplementary Material	Access the most recent supplemental material at: http://mct.aacrjournals.org/content/suppl/2021/07/20/1535-7163.MCT-21-0116.DC1

Cited articles	This article cites 33 articles, 12 of which you can access for free at: http://mct.aacrjournals.org/content/20/10/2008.full#ref-list-1

E-mail alerts	Sign up to receive free email-alerts related to this article or journal.
Reprints and Subscriptions	To order reprints of this article or to subscribe to the journal, contact the AACR Publications Department at pubs@aacr.org.
Permissions	To request permission to re-use all or part of this article, use this link http://mct.aacrjournals.org/content/20/10/2008. Click on "Request Permissions" which will take you to the Copyright Clearance Center's (CCC) Rightslink site.